

## Electrodeposition of Nano-Structured PbO<sub>2</sub> on Glassy Carbon Electrodes by FFT Continuous Cyclic Voltammetry

Tayebeh Mirzaei Garakani<sup>1</sup>, Parviz Norouzi<sup>1,2,\*</sup>, Majid Hamzehloo,<sup>3</sup> Mohammad Reza Ganjali<sup>1,2</sup>

<sup>1</sup> Center of Excellence in Electrochemistry, Department of Chemistry, University of Tehran, Tehran, Iran

<sup>2</sup> Endocrinology & Metabolism Research Center, Tehran University of Medical Sciences, Tehran, Iran

<sup>3</sup> Department of Physical Chemistry, Faculty of Chemistry, University of Tehran, Tehran, Iran

\* E-mail: [norouzi@khayam.ut.ac.ir](mailto:norouzi@khayam.ut.ac.ir)

Received: 30 November 2011 / Accepted: 21 December 2011 / Published: 1 January 2012

---

Nano-structured lead dioxide was prepared by an easy and fast continuous cyclic voltammetric technique. The prepared nano-structured lead dioxide films were ultimately aimed at producing cathodes with improved electrocatalytic activity and stability for the lead acid batteries. During the measurements, the potential waveform, which consisted of the potential step for electrodeposition and potential ramp, was continuously applied on a glassy carbon disk electrode. Different parameters such as step potential and its duration time, and also scan rate of continuous cyclic voltammetry were optimized to obtain higher capacity. Results comparison of the voltammetric experiments previously reported and those from laboratory-designed test cells have confirmed a higher charge/discharge performance of our electrodeposited samples towards the PbO<sub>2</sub>/PbSO<sub>4</sub> transformation in aqueous sulfuric acid solutions. The enhanced characteristics of this sample is attributed to its special morphology due to formation of nano structure at high scan rates, as confirmed by SEM. Maximum current efficiency was observed when step potential and time were equal to 1400mV and 1700ms, respectively, at a scan rate of 4000 mVs<sup>-1</sup>. Analysis of electrochemical impedance spectroscopy (EIS) data revealed that the charge transfer resistance is decreased by a change in scan rate as the FFT continuous cyclic voltammetric tests showed. A higher overpotential for oxygen evolution reaction was also observed for electrodes prepared in this electrochemical technique in sulfuric acid solution. The morphology of electrodeposited oxide are very different from those of oxide forming in lower scan rates, due to the high surface area obtained as well as high connectivity between particles resulted in increased discharge capacity.

---

**Keywords:** Electrodeposition, Lead dioxide, Fast continuous cyclic voltammetry, SEM

## 1. INTRODUCTION

Because of its commercial importance in lead-acid batteries, Lead dioxide electrodeposition is being an active research area [1–3]. Yet, the lead-acid battery system is more promising in applications to this field because of its low cost and vigorous nature [4, 5]. The PbO<sub>2</sub> 3-D nucleative growth pattern first studied on a Pt substrate [6] and then it has since been found to be similar on Pt [7], SnO<sub>2</sub> [8-10], glassy carbon [11-13], Au [14, 15] and glassy carbon and Pt microelectrodes [16, 17]. The effect of different electrolyte media such as NaOAc/HOAc [6], HBF<sub>4</sub> [7], HNO<sub>3</sub> [8] and HClO<sub>4</sub> [14], and even alkaline KOH [18] have been investigated for the PbO<sub>2</sub> deposition. PbO<sub>2</sub> electrodeposition can still be described, for nitrate solutions, by the following scheme [19]:



The first stage is the formation of oxygen-containing particles such as chemisorbed OH, followed by a chemical stage in which these species interact with the lead particles to form a soluble intermediate product, likely to contain Pb(III), which is then oxidized electrochemically creating a Pb(IV) soluble intermediate. Then, it is transformed into PbO<sub>2</sub> in a final chemical stage. According to this mechanism the growing rate of lead dioxide particles depends on the amount of the intermediate product formed during reaction (3) at the electrode surface. Correspondingly, any changes applied to the system should change the rate of PbO<sub>2</sub> electrodeposition probably due to an effect on the coverage by oxygen containing particles. There are many ways to produce oxide materials of this type are known, e.g., sol-gel techniques, plasmachemical method, etc. The electrochemical method should be distinguished as one of the most promising, which enables wide control over the composition and properties of composites because of its simple implementation and possibility of smoothly varying the technological parameters of the process [1,20–24]. It has been studied that the phase composition and morphology of lead dioxide formed electrochemically depend on various parameters such as substrate material, the electrochemical technique used and deposition conditions including acidic or basic media and presence of forming agent. Discharge performances of lead acid batteries are strongly limited by the positive plate and the related aging mechanism [25]. For instance, PbO<sub>2</sub> degradation could cause irreversible formation of lead sulfate in the active mass, short-circuits and grid corrosion processes. One of problems in charging/discharging of the electrode is decomposition of water which results to hydrogen and oxygen evolution through overcharging. Risk of explosion, corrosion of the grid alloys and water consumption will be increased by gas evolution enhancement. In order to reduce water consumption in maintenance free batteries the gas evolution overpotentials must be increased by different strategies reported in the literature [26–29]. Some of the electrochemical methods used to

fabricate lead dioxide include pulse current [30] constant current, constant potential [1] and cyclic voltammetry [1, 31]. As the influence of step potential on the electrochemical behavior of different systems is an active field of research [32-35], we decide to study the effect of this parameter on PbO<sub>2</sub> electrodeposition. Thus, Nano-structured lead dioxide was prepared by an easy and fast continuous cyclic voltammetric technique. The prepared nano-structured lead dioxide films were able to produce cathodes with improved electrocatalytic activity and stability for use in the lead acid batteries.

Electrochemical step (E<sub>s</sub>) permits the surface to be ready to form initiative nuclei and make the surface active for long periods of time. Additionally, in this method, the most important ability is applying a potential sweep at higher rate to increase the oxygen over potentials. The presented experiments describe a fundamentally different approach to PbO<sub>2</sub> synthesis on glassy carbon surface, in which the electrodeposition efficiencies are improved. Also, a preliminary study of the electrodeposition of lead dioxide as a function of scan rate at different step potential values has been carried out by means of a fast Fourier transformation continuous cyclic voltammetry (FFTCCV) analysis, with the results compared to those found in the literature [35]. The EIS and SEM techniques are, also, used to investigate the electrochemical properties of the prepared layer..

## 2. EXPERIMENTAL

All solutions used in the experiments were analytical reagents with the highest available purity and used without further purification. Lead nitrate (Pb(NO<sub>3</sub>)<sub>2</sub>), nitric acid (HNO<sub>3</sub>, 65%) and Sulfuric acid (H<sub>2</sub>SO<sub>4</sub>, 98%) were obtained from Merck Co. and all used as received. Double distilled water was used throughout all experiments. Lead dioxide was electrochemically deposited onto the disk area (diameter 1mm) of glassy carbon rod. The electrodes were polished to mirror finish with alumina powder (0.05 μm) and then rinsed with double distilled water several times before each experiment. After each experiment, the lead dioxide deposit was removed with 1:1 H<sub>2</sub>O<sub>2</sub>/Acetic acid followed by rinsing thoroughly with water. FFTCCV experiments process were performed in the solution, with the aid of a setup of a PC PIV Pentium with a data acquisition board (PCL818-HG, Advantech. Co.) and a custom made potentiostat described in our previous works [32-34] using a three-electrode arrangement of a glassy carbon (GC) working electrode, platinum wire auxiliary electrode and Ag/AgCl (KCl, saturated) reference electrode at a scan rate of 20 to 15000 mVs<sup>-1</sup>. A Luggin capillary with its tip set at a distance of 2mm from the surface of the working electrode was used to minimize the *iR* drop in the electrolytes. All data acquisition and data processing programs were performed in Delphi 6® program environment. The diagram of potential waveform applied during cyclic voltammetric measurements is shown in (Figure 1).

The potential waveform, which continuously applied on the electrode, involves two sections. First section is consisted one step applied before each potential ramp for electrodeposition of lead dioxide. Finally the current is measured during the potential ramp. Electrodeposition of the lead dioxide was performed on gc electrode from 10 ml electrolyte comprised 1M HNO<sub>3</sub>+ 0.1M (Pb(NO<sub>3</sub>)<sub>2</sub>), first at different time and potential of steps. The single-potential-step method of deposition involved stepping the potential to value nearby PbO<sub>2</sub> electrodeposition voltage which was held constant for a

very short time; typically 50 to 2500 ms, and subsequently the potential ramp is applied while the current was recorded. Then the electrodeposition of PbO<sub>2</sub> was carried out under applying optimum step potential with varying values of scan rates. All experiments were carried out at ambient temperature. As mentioned above, the current passing through the electrode was measured only during the potential ramp. At first, an electrode CV was recorded and then by applying FFT on the obtained data, the existing high frequency noises were pointed out. Finally, using this information, the cutoff the frequencies of the analog and digital filters were set at a specific value. This kind of filtration and also integration of the net current charges significantly reduces the noise level in the data obtained [36-41]. The current efficiency of the PbO<sub>2</sub> (CE<sub>PbO<sub>2</sub></sub>) and the PbO<sub>2</sub> electrodeposition current (I<sub>PbO<sub>2</sub></sub>) was obtained from equations:

$$CE_{PbO_2} = Q_{red}/Q \quad (6)$$

$$I_{PbO_2} = Q_{red}/t \quad (7)$$

Where Q is the total charge passed during the anodic polarization, Q<sub>red</sub> is the charge passed on PbO<sub>2</sub> reduction at E≈1300 mV and, t is the total time of the anodic polarization [19]. The electrodes prepared above were removed from their plating solution and carefully rinsed. These series of obtained electrodes, were introduced to FFTCCV experiments in a three-electrode cell containing H<sub>2</sub>SO<sub>4</sub> (0.5M) solutions. FFTCCV voltammograms were recorded at a scan rate of 100 mVs<sup>-1</sup> in the PbO<sub>2</sub>/PbSO<sub>4</sub> couple potential window of 500–2000 mV (e.g. 500 cycles were performed consecutively). The potential sweeps were initiated at the cell rest potential and scanned towards positive potentials versus reference electrode.

The AC impedance measurements were made as a function of frequency using an AUTOLAB system with PGSTAT30 and FRA2 boards (Eco Chemie, Utrecht, and The Netherlands). The system is run by a PC through FRA and GPES 4.9 software. The working electrode was prepared from a thin layer of PbO<sub>2</sub>. The same three electrode cell was used.

EIS tests were carried out in sulfuric acid 0.5 M, in the range of 100 kHz to 100mHz, at open circuit voltage (OCV) and 5mV potential amplitude. The impedance results was acquired and fitted by Zplot/Z-view software. Some charge/discharge experiments of PbO<sub>2</sub> samples were carried out in the same small undivided beaker cell using (an in-house developed, computer controlled charge–discharge and automated logging system) a laboratory constructed galvanostat controlled by a PC with an A/D interface and in-house written software.

During the “cycling series”, the cell was subjected to one charge/discharge cycle for electrodes prepared in both constant current and FFTCCV in an optimum potential step and scan rate. The cell voltage was measured directly using a data acquisition system. In the discharge experiments, the cell was discharged to a cut-off voltage of 1750 mV at a current density of 12 mAcm<sup>-2</sup>. Morphological studies of prepared samples were performed by means of SEM (Philips XL 30).

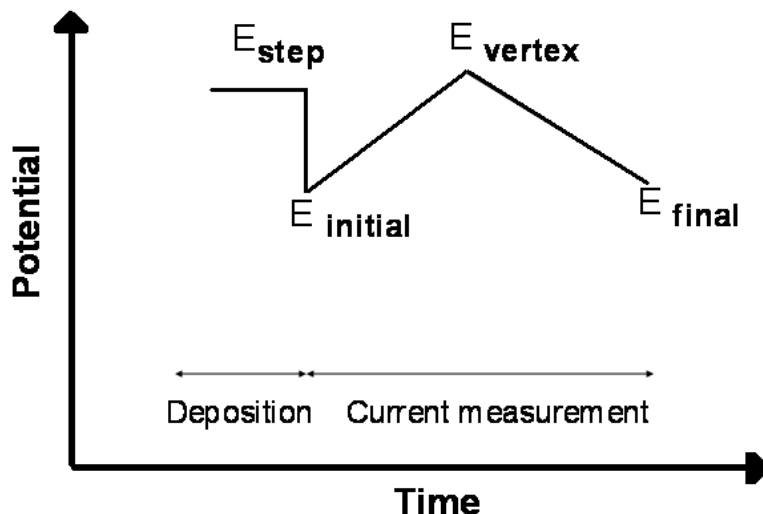


**Figure 1.** Diagram of the applied potential waveform for FFTCV method

As mentioned above, the nucleative process of  $\text{PbO}_2$  electrodeposition was conclusively established in an acidic media depends on some pretreatment applying on the surface. During the experiments, the current passing through the electrode was sampled only during the potential ramp and data processing operation is carried out in parallel with data acquisition during experiments. The integration of net current changes is applied over the selected scanned potential range.

### 3. RESULTS AND DISCUSSION

#### 3.1. Investigation of applying step potential effect on thin film $\text{PbO}_2$ synthesis

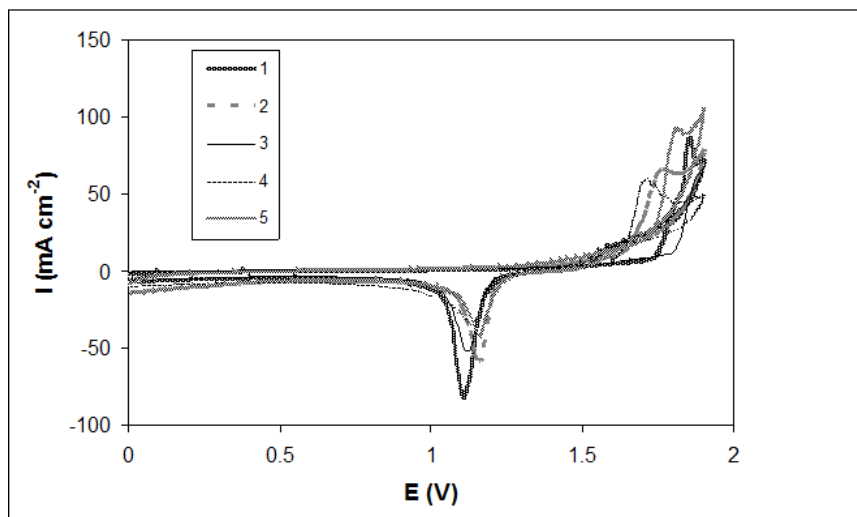
(Figure 2a) shows the recorded cyclic voltammograms of GC electrode in 1 M  $\text{HNO}_3$  and 0.1 M  $\text{Pb}(\text{NO}_3)_2$  by applying various step potentials (for 1700 ms in the scan rate of  $100 \text{ mVs}^{-1}$ ). These voltammograms shows the effect of initial potential step (before potential scan) on formation of the oxide layer on the electrode surface. The fairly large number of electrodeposition methods for preparing the lead dioxide film reported earlier [1, 30, 31] along with some measurements carried out on different media. It is worth to note this fact that the medium with all its variation of pH and anions just was used as a source of  $\text{Pb}^{2+}$  ions and that it does not affect nucleation process by adsorption or any related surface process [42]. So the medium of  $\text{HNO}_3$  and  $\text{PbNO}_3$  in their mentioned concentration was chosen to allow comparison of our results with those was obtained on the same surface [35]. The changes in the both cathodic and anodic peaks, suggests that the potential step can improve the oxide layer formation by the building up of a compact  $\text{PbO}_2$  deposit consisting of  $\text{PbO}_2$  nuclei, which can strongly adhered to the electrode surface. Consequently, the exposed surface area of  $\text{PbO}_2$  for cathodic dissolution decreases and hence the peak current of  $\text{PbO}_2$  reduction increases. This may indicates the increase in effective surface area for further growth also causes lower nucleation overvoltage and shift

of peak potential (curves 1 to 3), again to more negative values at steady-state conditions (curve 4). However, in the absence of step potential within the same media, the smaller crystallites and amorphous phases continue to dissolve chemically. Hence, small-sized crystallites would not be available for further growth during the anodic potential ramp, only a few large-sized crystals that escaped chemical dissolution would be available for growth and therefore a lower  $Q$  is obtained.

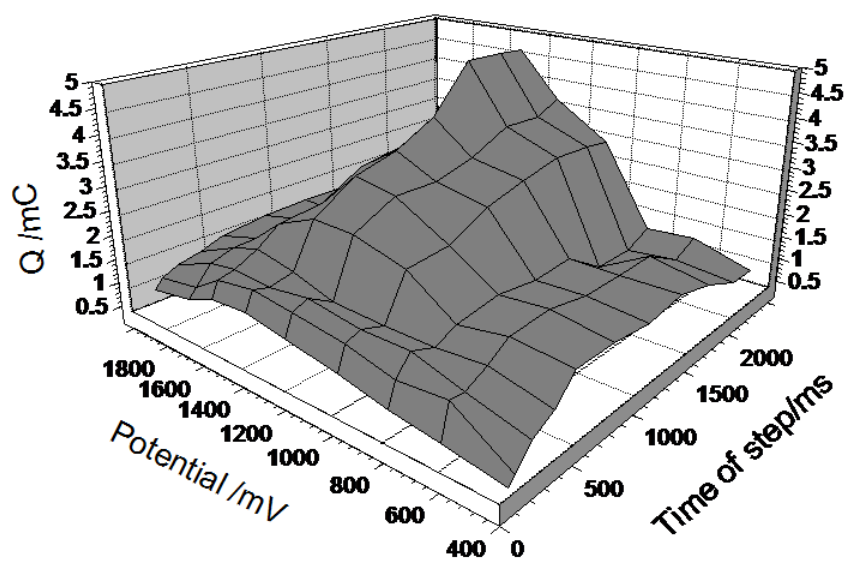
For achieving the best time and potential step, the amount of total charge (for potentials 400 to 2000 mV) at is calculated and time steps of 50 to 2500 ms (potential range of 1100 to 1300 mV). (Figure 2b) shows the effect of the step parameters (time duration and potential) on the  $Q$  of the cathodic peak current. As shown in Fig. 2a the rising portions of the cathodic current correspond to a process of growth taking place during the application of the step potential. It can be noticed that by increasing the potential and time of the potential step the cathodic peak increases, which is of indication of larger amount of oxide layer (so the charge under this peak used for optimizing the deposition parameters). Furthermore, the graph shows that the time of the potential step up to 1700 ms improves the deposition process, and seems to have no significant effect at longer time on the process. Also, the best potential step is 1400 mV. In fact, since the potential of zero charge of lead dioxide in 1M  $\text{HNO}_3$  is around  $0.91 \pm 0.1\text{V}$  [43], at the deposition potentials ( $E > 1400\text{ mV}$ ) the electrode surface will be positively charged, and may the latter deposition leads to a more unstable layers.

(Figure 2c) and d, shows SEM images of the surface morphologies at 1600 and 1400mV potential of the step and it can be concluded that with the deposit forms at potential scan rate of  $100\text{ mVs}^{-1}$ , there are many holes and cracks on the prepared layer making the surface nonuniform. This appearance is presumably the result of gas evolution damage (Figure 2c). In fact, the damage is minor by applying step potential at 1400 mV (and is very significant at potential near 1800 mV). Consequently it can be observed that under optimum condition of applied step potential, the deposits were uniform and compact enough to strongly adhere on the GC electrode surface with an almost 'ceramic' appearance as confirmed by obtained cyclic voltammograms and the calculated cathodic charge is represented in (Figure 2b). At step potential of 1800 mV, there would be an increase in labile oxygen creation and it may hold back the chemisorbed OH production, which is indirectly can be responsible for producing  $\text{PbO}_2$  [44]. Therefore, such defects could be observed within the bulk of active material in the form of large cracks and pores due to evolution of bigger oxygen bubbles and dissolution of  $\text{PbO}_2$  within the active material resulting in nonuniformity of the obtained the oxide layer. Also, some electrochemical failures such as, decrease in the effective electrical conductivity of the layer (which may inhabit a good electron flow across these huge fractures) can have contribution in creating these defects. This may help to interpret the decrease in  $Q$  at step potentials higher than 1600 mV shown in (Figure 2b).

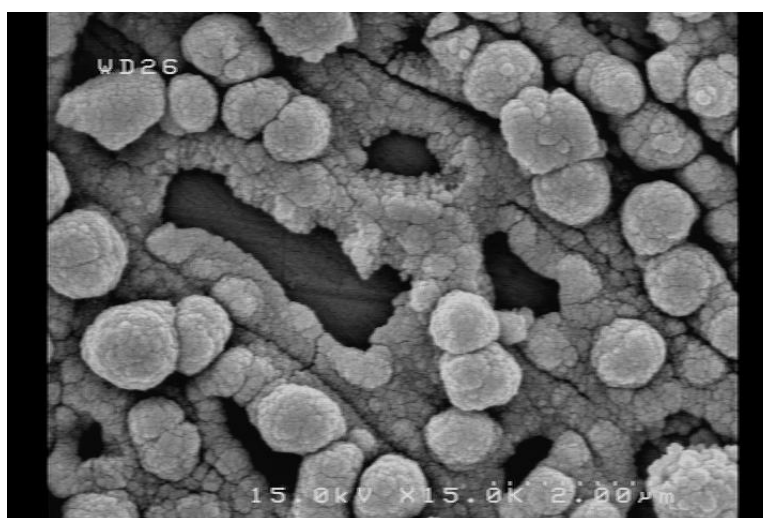
Moreover, it can be say that by applying the step potential at the optimum value, the surface concentration of the oxygen species is increased enough that are more strongly bonded to the electrode surface [35]. This speculation is consistent with equations 2 to 5, showed that the rate of lead dioxide formation will increase with an increase in the  $(\text{OH})_{\text{ads}}$  bond strength with electrode surface or, with a decrease in the amount of labile oxygen particles. As a result, by going to higher potentials those species are oxidized to  $\text{O}_2$  and gas evolution carried out on the electrode as well as  $\text{PbO}_2$  electrodeposition.



(a)



(b)



(c)

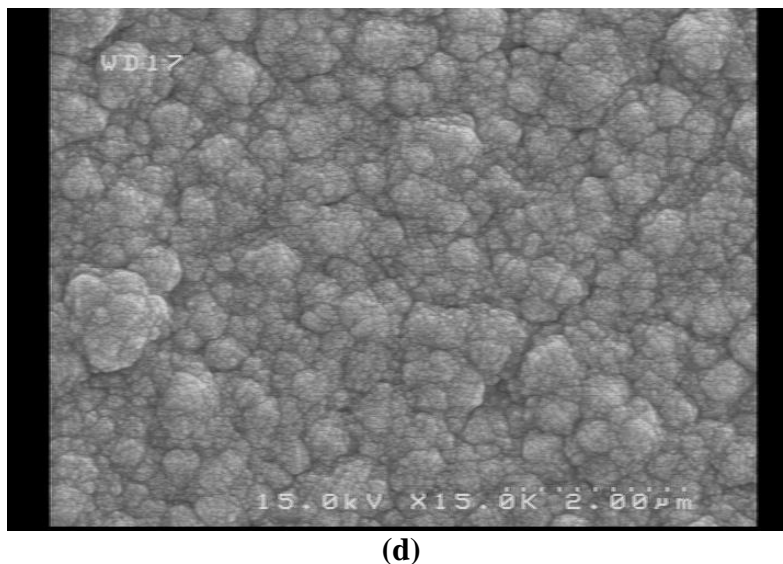


**Figure 2.** a) Cyclic voltammograms of GC electrode in 1 M HNO<sub>3</sub> and 0.1 M Pb(NO<sub>3</sub>)<sub>2</sub> by applying step potentials (for 1700 ms) in the scan rate of 100 mVs<sup>-1</sup> (shown in Fig.1): (1) 1400 mV, 2) 800 mV,(3) 1200mV, (4) 1600mV, (5) without applying any potential step, b: The effect of step time and potential on formation of the oxide layer, which was used for optimization; c) SEM of deposited PbO<sub>2</sub> at step potential of 1600 mV and, d) 1400 mV.

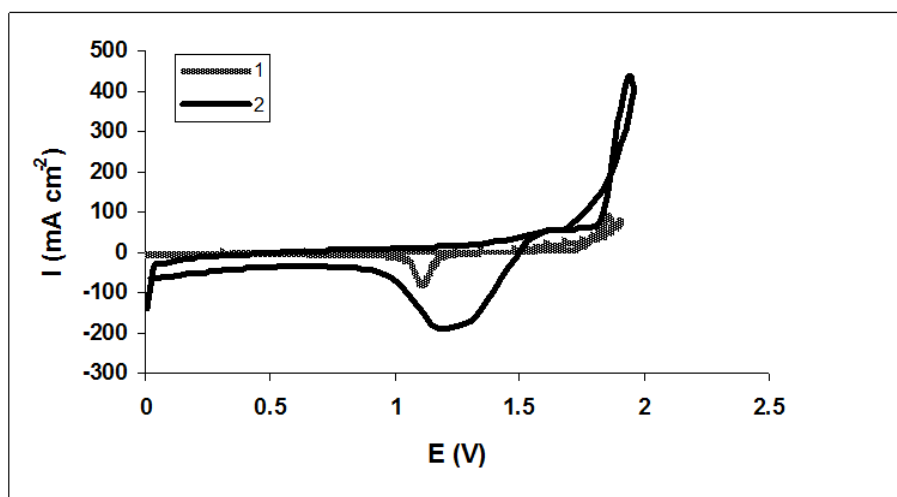
### 3.2. Study of residual nuclei and their growth by varying the potential scan rate.

#### 3.2.1. FFTCCV study.

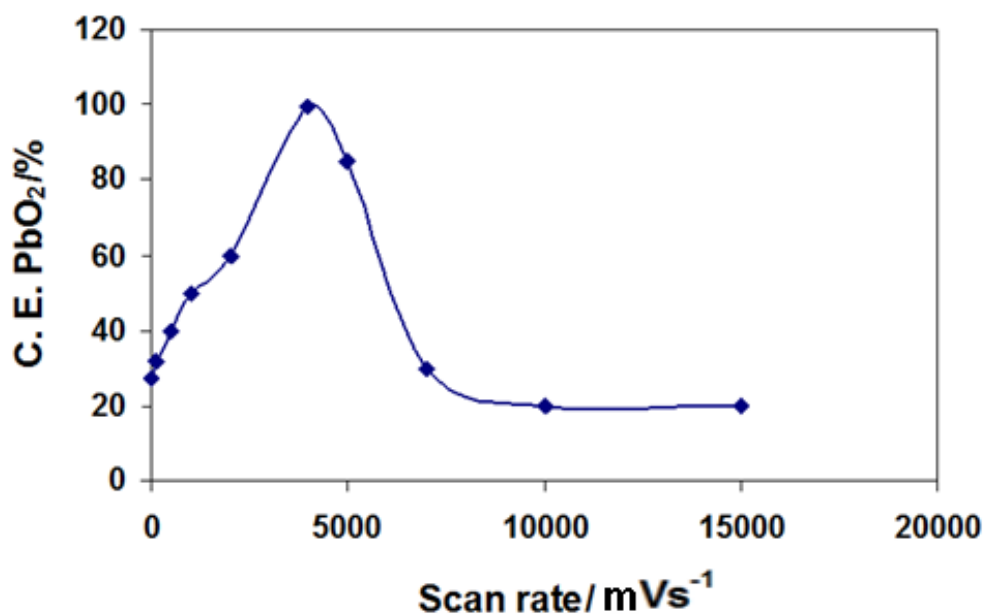
(Figure 3a) shows single FFTCCVs of GC electrode in solution nitric acid (1M) and lead nitrate (0.1 M) at two different potential scan rates for PbO<sub>2</sub> formation (at optimum values of the time and potential step). This figure shows the enhancement of the cathodic current increases by increasing the scan rate, which is an indication of a better electrodeposition of PbO<sub>2</sub>. This, also, conformed by measuring current efficiency of PbO<sub>2</sub> electrodeposition (Figure 3b), which suggests the optimum value for the scan rate is 4000 mVs<sup>-1</sup>. As previously reported [42], the charge consumed during the cathodic process (Q<sub>c</sub>) is always less than the charge consumed during the anodic process (Q). Consequently the Q<sub>c</sub>/Q is found to be around 0.8 or even less in all previous experiments. The Q<sub>c</sub>/Q value rise to tremendously high values (around 0.9 and more) in this work, at optimum applying conditions and after 500 cycles. It is established that in this the voltammetric measurements the reduction of PbO<sub>2</sub> crystallites is always incomplete [42]. However, chemical dissolution of PbO<sub>2</sub> formed in acidic medium may be the main cause for the extremely low Q<sub>c</sub>/Q values at low scan rates.

The residual PbO<sub>2</sub> growth was created by using continuous cyclic voltammetry experiments. In (Figure 4) the three dimensional graphs show FFTCCV in potential range of 0 to 2000 mV at two scan rates, during PbO<sub>2</sub> electrodeposition on the GC electrode, in which the cycled up to about 5000 at optimum potential step. These three dimensional graphs more clearly shows the influence of residual PbO<sub>2</sub> crystals formed from the applied potential step on the further growth of PbO<sub>2</sub> on second and subsequent sweeps in comparison with data reported before [35]. It was found that low scan rate (100

$\text{mVs}^{-1}$ ) by cycling the electrode, the cathodic peaks decline significantly, in contrast, at potential high scan rate ( $4000 \text{ mVs}^{-1}$ ), the cathodic peak increases and then it grows very slowly. This phenomenon can be attributed to particles instability at the electrode surface at low scan rates as a result of the particles aggregation during potential sweeps. Moreover, increasing the scan rate can be the result of enhance of the surface sites that able to absorb hydroxyl, according to the mechanisms mentioned in last section (equ. 2-5).



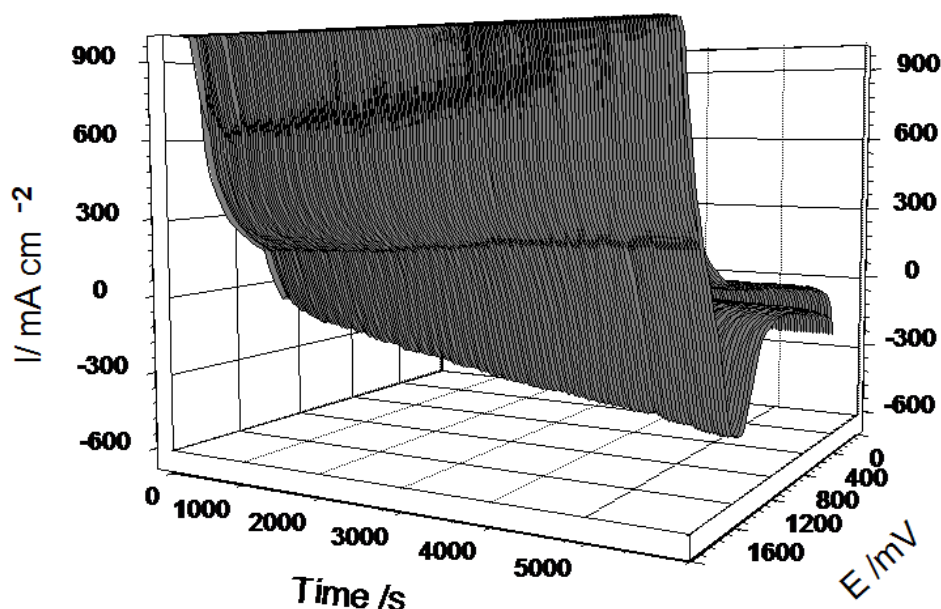
(a)



(b)

**Figure 3.** FFT cyclic voltammogram of GC electrode in 1 M  $\text{HNO}_3$  and 0.1 M  $\text{Pb}(\text{NO}_3)_2$  at two scan rates of (1) 100 (2)  $4000 \text{ mVs}^{-1}$ ; b) Lead dioxide yields at GC electrode in the same solution at different scan rates after 500 cycles.

The large cathodic peak current at  $4000 \text{ mVs}^{-1}$  suggests the fact that the growing phase on the electrode surface consists only of more uniform layer made up crystallites, which is similar to porous layer essentially in its nature and the electrolyte can move through the pores during the potential ramp. Electro-reduction proces in the porous inner regions is still possible and hence higher cathodic currents are noticed in the subsequent sweeps as well [35, 43, 45]. For that reason, the cathodic peak area for electrodeposition of lead dioxide increases. Since the surface area available for growth slowly increases with the number of sweeps, the steady-state peak current also increases steadily (Figure 4) to reach a maximum value after a number of potential scans.



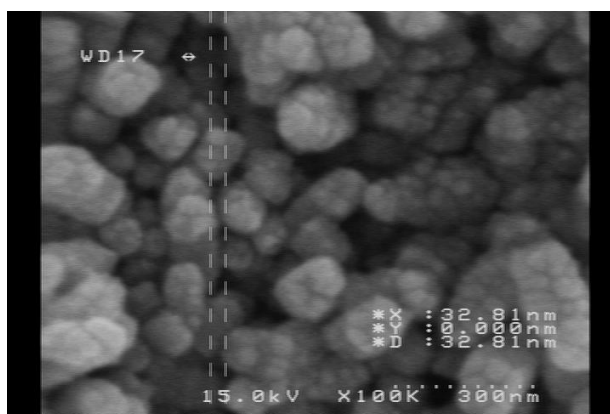
**Figure 4.** FFTCCV of GC electrode in  $1 \text{ M HNO}_3/0.1 \text{ M Pb(NO}_3)_2$ , scan rate  $4000 \text{ mVs}^{-1}$ .

Figure 5a shows the layer deposited at  $4000 \text{ mVs}^{-1}$  is well oriented and has nanostructure. This can explain the larger value of  $Q_c$  that observe at the voltammetric response at this scan rate. Existence of such nanoparticles on the electrode indicates the formation of  $\text{PbO}_2$  nuclei at the potential step with less oxygen gas interference. It seems that presence of a large number of  $\text{PbO}_2$  nuclei at  $4000 \text{ mVs}^{-1}$  acts as substrate for its further electrodeposition with less energy consumption. One can observe during subsequent voltammetric sweeps results cathodic current improvement From the micrographs can be seen that the nuclei are growing close to cylindrical shape, and the size distribution suggests varying ages of the nuclei. The small apparent distortion from sphericity can be due to the angle of the sample.

At low scan rate with formation of unstable  $\text{PbO}_2$  deposit due to the intense effect of oxygen evolution, the surface becomes nonuniform and finally there would not remain an uniform layer on the surface because of the dissolution. Figure 5b is  $\text{PbO}_2$  layer with very uniform structure compare to (Figure 5a). As is noticeable from Figure 5b, the obtained samples by FFTCCV method, at high

potential scan rate, are relatively same size and distributed along the observed uniform PbO<sub>2</sub>. These features are in agreement with the evidence from current transients, which correspond to progressive nucleation and growth of three-dimensional cultures [13, 42]. On the other hand, figure 5b shows that the deposit is mainly localized in two circular regions and some areas near the edges, where the crystallites appear to be aligned along preferential directions, and a notable feature is the absence of faceting at this stage of growth.

A close-up view of the circular region showed random nucleation and growth of spherical nuclei. Thus, from the results obtained two important effects should be noticed in the multisweep cyclic voltammograms, which are responsible for an increase in value for Q<sub>c</sub> at high scan rate in the process of PbO<sub>2</sub> deposition. It can be propose that at high scan rates (or at low windows times) a small number of tiny oxygen bubbles can be created at the electrode surface (at very positive potentials), which can results fine pores in the electrodeposited PbO<sub>2</sub> layer. In this case, nano pores can surround the deposited lead dioxide particles and limit their further growth and, consequently, the particle's dimension is decreased.



(a)



(b)

**Figure 5.** SEM images of lead dioxide samples synthesized by (a) continuous cyclic voltammetry at the scan rate of 4000 mVs<sup>-1</sup>. and (b) 100 mVs<sup>-1</sup>.

In addition, it seems that there would lack of time for the growth of  $\text{PbO}_2$  nuclei at higher scan rates than  $4000 \text{ mVs}^{-1}$ , consequently,  $Q_c$  becomes smaller due to limitations in kinetic process of  $\text{PbO}_2$  reduction. These observations lend support to the influence of residual nuclei, which are remained on the surface from previous potential steps. It can be suggested that, at high scan rates, the nucleation rate exceeds the rate of nuclei growth. Also, at this scan rate, nucleation rate is suitable in order to synthesize nanoparticles in a uniform pattern. In contrast, at low scan rates, nuclei growth is high and the lead dioxide crystals grow irregularly to make the surface less effective.

### 3.2.2. EIS study.

As it has been clarified elsewhere [45, 46], EIS was a convenient technique to characterize the electrical properties of coatings and their adhesion to metal surfaces conforming the battery results. This way is helpful to give information about potential dependence of coverage by adsorbed  $\text{PbO}_2$  electrodeposition intermediate. The obtained Nyquist plots  $\text{PbO}_2$  film in  $0.5\text{M H}_2\text{SO}_4$  solution at open circuit potential (performed at  $1300 \text{ mV}$ ) formed electrochemically are shown in Figure 6.  $\text{PbO}_2$  was electrodeposited on GC electrodes from a solution containing  $0.1\text{M Pb}(\text{NO}_3)_2$ ,  $1\text{M HNO}_3$ , in three conditions. EIS was employed to evaluate the electrochemical performance of the obtained layers. In the Nyquist plots, there is a straight line at low frequencies, which is almost dependent on the scan rate used for depositing  $\text{PbO}_2$  and also applying step potential. The high frequency region of the spectra is characterized by a semicircle, which is slightly depressed. These results show a porous electrode [46,47].

The impedance spectra for  $\text{PbO}_2$  prepared at a scan rate of  $100 \text{ mVs}^{-1}$  is shown in (Figure 6a). The result can be fitted well by the equivalent circuit included. Semicircle diameter is a measure of charge transfer resistance at the kinetic controlled zone of Nyquist plot. Accordingly, it is revealed that the charge transfer resistance for  $\text{PbO}_2$  forming at high scan rate is lower than that of formed  $\text{PbO}_2$  at lower scan rates (both by applying the same step potential), as expected by regarding of discharge capacities of these batteries (see the next section). These EIS results are, also, consistent with the results obtained from the FFTCCV studies. They conform that  $\text{PbO}_2$  prepared with the optimal potential step ( $1400\text{mV}$ ) at low scan rate, possess a lower internal resistance and so higher redox peak current (capacity) compare to the layer obtained by applying no step potential at the same scan rate. This figure, also, indicates that the resistance of the electrolyte for  $\text{PbO}_2$  formed in conditions describing above, in  $\text{H}_2\text{SO}_4$  solution is independent of the applied step potential and also the varying of scan rate. As mentioned above, the  $\text{PbO}_2$  nanoparticles are distributed homogeneously as the particles diffuse from high to low concentration regions. Increasing the scan rate yields a higher diffusion rate, which appears to be beneficial to make more uniform  $\text{PbO}_2$  nanoparticles. A proposed equivalent circuit has been shown in (Figure 7) which is similar to those developed in some previous articles [46, 47,48]. The interpretation of the physical elements of the proposed equivalent circuit is similar to those reported in previous study [48]. As can be concluded from Nyquist plots in (Figure 6), three electrodes synthesized at different conditions consist of a semicircle part, which shows a kinetic controlled behavior of the system. The morphology of electrode prepared at optimum condition shows a high porous skeleton structure, which facilitate the penetration of electrolyte to sub layer active sites. In fact

a low capacity of lead acid battery can arise from the low connectivity between particles at low scan rates. As it has been shown by Petersson et al. [49], the observed resistance divided into two categories, one is ohmic resistance due to electrolyte resistance and degree of contact between the lead dioxide particles in the obtained layer. Another part of resistance is pore resistance, which can be observed because of porous structure of the oxide layer. Differences between the Nyquist plots arising from layer thickness values. Also, difference in semicircle diameter for these plots revealed different porosity of oxide layers obtained at dissimilar conditions. It is obvious that the oxide electrode prepared by applying the step potential of 1400mV for duration time of 1700 ms at the scan rate of  $4000 \text{ mVs}^{-1}$  shows lower ohmic resistance. It is probably due to more porous and lesser thickness  $\text{PbO}_2$  layer.

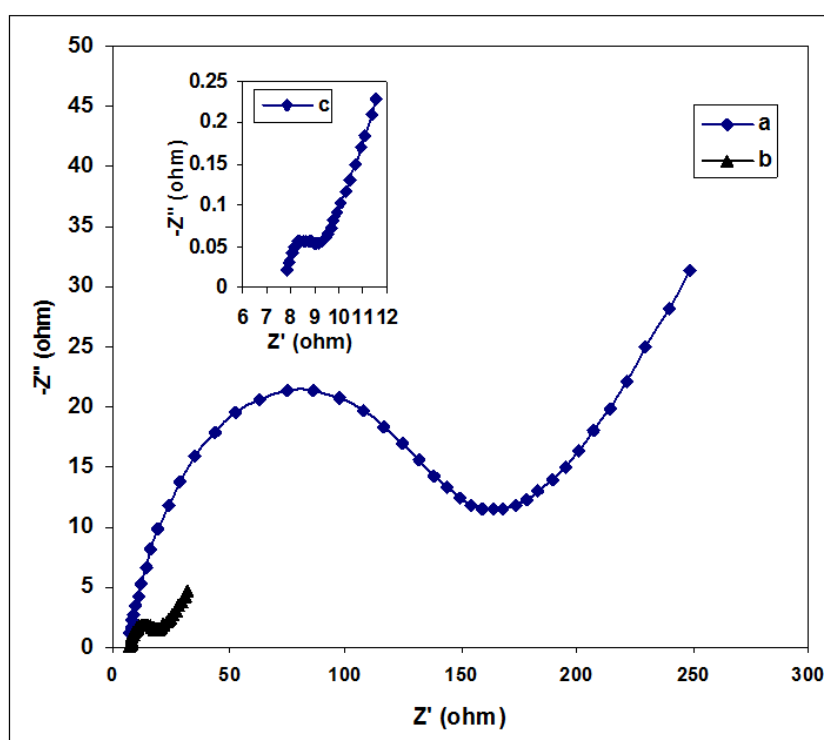


**Figure 6.** EIS of samples prepared in 1 M  $\text{HNO}_3/0.1 \text{ M Pb}(\text{NO}_3)_2$  at scan rates of a)  $100 \text{ mVs}^{-1}$  without applying any steps b)  $100 \text{ mVs}^{-1}$  at step potential and time of 1400mV and 1700ms and c)  $4000 \text{ mVs}^{-1}$  at step potential and time of 1400mV and 1700ms. Impedance experiments were carried out in 0.5M sulfuric acid at open circuit voltage vs.  $\text{Ag}/\text{AgCl}$  (KCl, saturated).

This observation, also, verifies the interpretation of the effect of step potential applied within  $\text{PbO}_2$  electrodeposition and FFTCCV measurements in previous section. In addition, decrease in semicircle radius due to porous structure of the oxide layer could be observed and described by a constant phase element, CPE [48,50]. Since there are  $\text{PbSO}_4$  crystals on the surface of prepared  $\text{PbO}_2$ , a large charge transfer resistance was observed, which leads to a lower discharge capacity. Complex plots are observed at figures 6a and b that are consisting of a semicircle at higher frequency with a  $45^\circ$  sloping line at low frequency indicating the presence of a kinetic and diffusion controlled process [48,

49]. For the  $\text{PbO}_2$  (prepared at high scan rate) the observed shape of the AC impedance spectra (Figure 6c) indicates that the electrochemically processes are more kinetically controlled, rather than diffusion controlled. The gradual increase in the value of  $C_{dl}$  from conditions described in (Figure 6a) to c, can be due to solution penetration between the coating and GC surface. This penetration can be through small breakdown sites of the coating.

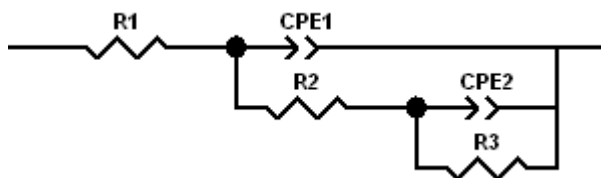


**Figure 7.** Equivalent circuit used to obtain impedance parameters for (the  $\text{PbO}_2$ ) with the ZView<sup>®</sup> software.

### 3.3. The behavior of obtained $\text{PbO}_2$ in $\text{H}_2\text{SO}_4$ and discharge capacity

Cyclic voltammetry has been used extensively to characterize the behavior of lead dioxide in sulphuric acid [51-55], but there is no comparison of successive behavior of obtained  $\text{PbO}_2$  in this media. Nevertheless, it is useful to compare the current densities observed with  $\text{PbO}_2$  surfaces prepared by two different methods in long period of time. During the reverse sweep, an anodic current is observed for  $E > 1700$  mV (recovery of lead dioxide by the oxidation of the lead sulfate formed during the previous reduction step). Also by comparison the FFTCCV of obtained electrodes in  $\text{H}_2\text{SO}_4$ , it can be concluded that after 6000s the cathodic peak current ( $I \approx 8$  mA) for the electrode prepared by the FFTCCV method is higher than cathodic peak current ( $I \approx 0$  mA) of  $\text{PbO}_2$  prepared by the constant current method (for  $\text{PbO}_2$  that prepared at constant current of  $10 \text{ mAcm}^{-2}$ ). For  $\text{PbO}_2$  prepared in constant current, the cathodic current excursions observed in the  $\text{PbO}_2/\text{PbSO}_4$  region on the reverse sweep appear only on the first few cycles. The FFTCCV voltammograms of  $\text{PbO}_2$  obtained at higher scan rate shows not only a decrease in cathodic peak due to sulphate formation, but also typical structure in the region where  $\text{PbO}_2$  is formed and subsequently reduced is always available.

In the case of lead dioxide obtained at  $4000 \text{ mVs}^{-1}$ , the porosity of the  $\text{PbO}_2$  layers due to evolution of very small size of  $\text{O}_2$  bubbles during electrodeposition mentioned earlier can help  $\text{H}_2\text{SO}_4$  to penetrate to the interior layers, which can cause more active sites are available to interact. As results, the intensity of the corresponding oxidation and reduction peaks increase until a significant steady state peak appears, which is as a result of saturation of nano pores by  $\text{H}_2\text{SO}_4$  as shown in (Figure 8b) [31, 48]. Therefore, the total amount of active mass involved in the electrochemical reaction increases in the first few scans [31, 49]. Consequently, the service life of the film obtained by FFTCCV mode at optimum high scan rate and step potential will be much longer than that in the other method.

As obvious from (Figure 8a) the following strong current suppression seems to be due to reduced diffusivity of the protons into the  $\text{PbO}_2$  crystal lattice (less porosity in the layers by the

constant current electrodeposition method) and/or more passivation of electrode through the formed  $\text{PbSO}_4$  [45,56]. Then the prepared electrodes were used as cathode of the lead acid batteries.

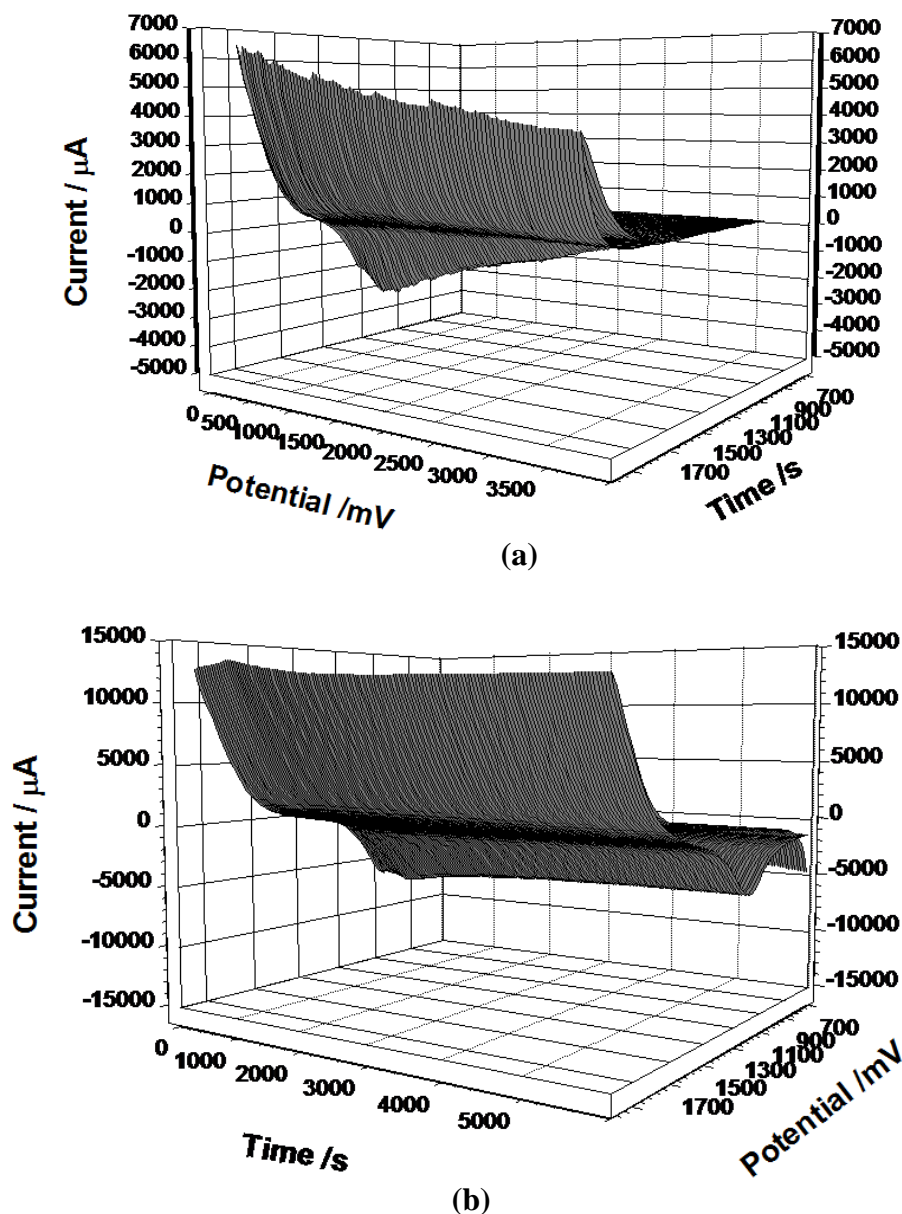


**Figure 8.** a) FFTCCV of  $\text{PbO}_2$  sample carried out in  $\text{H}_2\text{SO}_4$  solution (0.5M), scan rate,  $100\text{mVs}^{-1}$ . Lead dioxides were electrodeposited in 1 M  $\text{HNO}_3/0.1$  M  $\text{Pb}(\text{NO}_3)_2$  a) at constant current of  $10\text{mA cm}^{-2}$  and b) by FFTCCV method at scan rate of  $4000\text{ mVs}^{-1}$

The effect of discharge current density on the capacity of the battery prepared with sample obtained at optimum condition was examined (the inset of (Figure 9)). This figure shows maximum capacity was observed when a current density of  $12\text{mAcm}^{-2}$  was applied for discharge of the battery. At higher current densities, only the outer layer of the electroactive material can contribute to the discharge process and a lower capacity was achieved [45, 52]. As a result, this current density was

selected for discharge of the battery. The battery with positive electrodes obtained by two different methods was discharged at constant current of  $12\text{mAcm}^{-2}$ . The time-voltage behaviors of the battery during discharge process were shown in (Figure 9). As it is obvious, the discharge time for the battery assembled with cathode obtained by FFTCCV at high scan rate is more than other. It can be concluded that this battery has higher capacity, energy density and power.

Based on the results obtained from figures 8 and 9, it can be concluded that there is a good correlation between the FFTCCV of obtained  $\text{PbO}_2$  layer in  $\text{H}_2\text{SO}_4$  and discharge behavior of the samples examined in the same media. The significant factor involved in producing a cathode with high discharge capacity is access to sites of reaction [45-48]. Therefore, the electrodes containing enough porosity and large surface area can provide these conditions. These obtained data are in consistent with FFTCCV data achieved of  $\text{PbO}_2$  electrodeposited at high scan rate by applying step potential at its optimum value. Thus, the electrodeposition technique studied can be recommended for use as electrodeposition method with a prolonged service life. Further studies would be worthwhile.

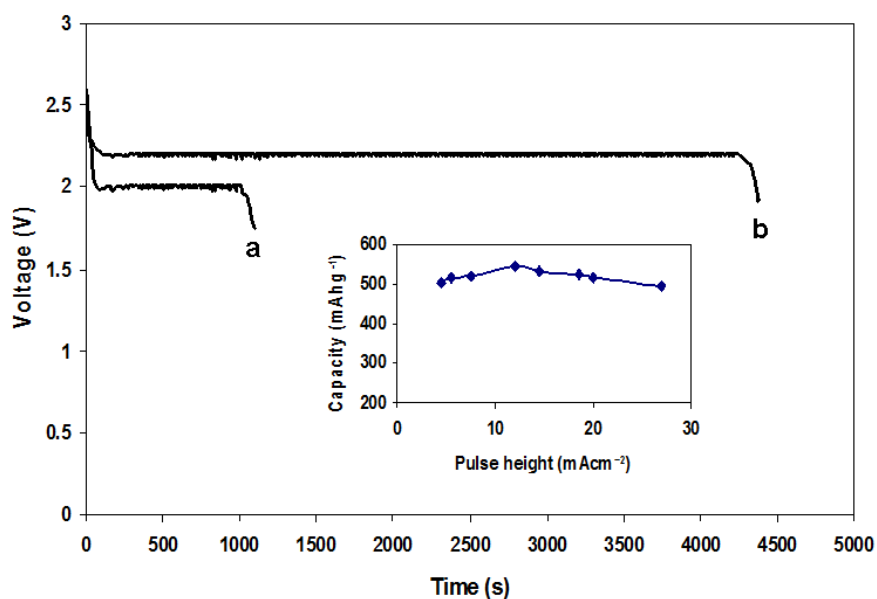


**Figure 9.** Time-voltage behavior of the batteries which prepared in  $1\text{ M HNO}_3/0.1\text{ M Pb}(\text{NO}_3)_2$  a) at constant current of  $10\text{mA cm}^{-2}$  and b) by FFTCCV method at scan rate of  $4000\text{ mVs}^{-1}$ , discharge current is  $12\text{mAcm}^{-2}$ . The inset is effect of discharge current density on capacity of samples prepared at the scan rate of  $4000\text{ mVs}^{-1}$  at step potential and time of  $1400\text{ mV}$  and  $1700\text{ ms}$  respectively in the electrolyte of  $4.8\text{M H}_2\text{SO}_4$ .

#### 4. CONCLUSION

In this work, FFTCV technique was used for the preparation of nano-structured lead dioxide at GC electrode. The lead dioxide films prepared were ultimately aimed at producing cathodes with improved electrocatalytic activity and stability for lead acid batteries. Different parameters such as step potential and its duration time, and also scan rate of FFTCCV were optimized to obtain higher

capacity. The enhanced characteristics of this sample is attributed to its special morphology due to the formation of nano-structure at high scan rates, as confirmed by SEM. Maximum current efficiency was observed when step potential and time were equal to 1400mV and 1700ms, respectively, at a scan rate of 4000 mVs<sup>-1</sup>. Analysis of EIS data revealed that the charge transfer resistance is decreased by a change in scan rate.

## References

1. P.K. Shen and X.L. Wei, *Electrochim. Acta*, 48 (2003) 1743
2. A.B. Velichenko, R. Amadelli, A. Benedetti, D.V. Girenko, S.V. Kovalyov and F.I. Danilov, *J. Electrochem. Soc.* 149 (2002) C445
3. S. Abaci, K. Pekmez, T. H€okelek and A. Yildiz, *J. Power Sources* 534 (2002) 1
4. P. Van den Bossche, F. Vergels, J. Van Mierlo, J. Matheys and W. Van Autenboer, *J. Power Sources*, 162 (2006) 913
5. P.T. Moseley, B. Bonnet, A. Cooper and M.J. Kellaway, *J. Power Sources* 174 (2007) 49
6. M. Fleischmann and M. Liler, *Trans. Faraady Soc.*, 54 (1958) 1370
7. F. Beck, *J. electroanal. Chem.* 65 (1975) 231
8. J.T. Kinard and R.C. Propst, *Anal. Chem.* 46 (1974) 1106
9. H.A. Laitinen and N.H. Watkins, *Anal. Chem.* 47 (1975) 1352
10. H.A. Laitinen and N.H. Watkins, *J. Electrochem. Soc.*, 123 (1976) 804
11. R.G. Barradas and A.Q. Contractor, *J. Electroanal. Chem.* 129 (1981) 327
12. R.G. Barradas and A.Q. Contractor, *J. Electroanal. Chem.* 138 (1982) 425
13. A.C. Ramamurthy and T. Kuwana, *J. Electroanal. Chem.* 13 (1982) 243
14. H. Chang and D.C. Johnson, *J. Electrochem. Soc.* 136 (1989) 17
15. H. Chang and D.C. Johnson, *J. Electrochem. Soc.*, 136 (1989) 23
16. L.J. Li, M. Fleischmann and L.M. Peter, *Electrochim. Acta*, 34 (1989) 459
17. L.J. Li, M. Fleischmann and L.M. Peter, *Electrochim. Acta*, 34 (1989) 475
18. N. Munichandraiah and S. Sathyanarayana, *J. Appl. Electrochem.*, 1 (1988) 314
19. A.B. Velichenko, R. Amadelli, E.A. Baranova, D.V. Girenko, F.I. Danilov, *J. Electroanal. Chem.*, 527 (2002) 49
20. S. Cattarin and M. Musiani, *Electrochim. Acta* 52 (2006) 1339
21. U. Casellato, S. Cattarin, P. Guerriero and M. Musiani, *Chem. Mater.*, 9 (1997) 960
22. M. Shiotu, T. Kameda, K. Matsui, N. Hirai and T. Tanaka, *J. Power Sources*, 144 (2005) 358
23. Q.T. Vu, M. Pavlik, N. Hebestreit, J. Pflieger, U. Rammelt and W. Plieth, *Electrochim. Acta*, 51 (2005) 1117
24. S. Cattarin, I. Frateur, P. Guerriero and M. Musiani, *Electrochim. Acta* 45 (2000) 2279
25. P. Ruetschi, *J. Power Sources* 127 (2004) 33
26. N. Bui, P. Mattesco, P. Simon, J. Steinmetz and E. Rocca, *J. Power Sources*, 67 (1997) 61
27. S.G. Hibbins, F.A. Timpano, D.J. Zuliani, *US Patent no.*, 5 (1996) 547
28. C. Francia, M. Maja and P. Spinelli, *J. Power Sources*, 95 (2001) 119
29. D. Pavlov, *J. Power Sources* 42 (1993) 345
30. N. Vastistas and S. Cristofaro, *Electrochem. Commun.*, 2 (2000) 334
31. D. Devilliers, M.T. Dinh Thi, E. Mah' e, V. Dauriac and N. Lequeux, *J. Electroanal. Chem.* 573 (2004) 227
32. P. Norouzi, H. Rashedi, T. Mirzaei Garakani, R. Mirshafian and M.R. Ganjali, *Int. J. Electrochem. Sci.*, 5 (2010) 377
33. P. Norouzi, M.R. Ganjali, S. Shirvani-Arani, A. Mohammadi, *J. Pharm. Sci.* 96 (2007) 893

34. M.R. Ganjali, P. Norouzi, R. Dinarvand, R. Farrokhi and A.A. Moosavi-movahedi, *Mater. Sci. Eng. C*, 28 (2008) 1311
35. V. Sáez, E. Marchante, M.I. Díez, M.D. Esclapez, P. Bonete, T. Lana-Villarreal, J. González García and J. Mostany, *Materials Chemistry and Physics*, 125 (2011) 46
36. P. Norouzi, T. Mirzaei Garakani, H. Rashedi, H.A. Zamani and M.R. Ganjali, *Int. J. Electrochem. Sci*, 5 (2010) 639
37. P. Norouzi, M. Qomi, A. Nemati and M.R. Ganjali, *Int. J. Electrochem. Sci*, 4 (2009) 1248
38. P. Norouzi, M. R. Ganjali, and L. Hajiaghababaei, *Anal. Lett.*, 39 (2006) 1941
39. P. Norouzi, M.R. Ganjali, A. Sepehri, and M. Ghorbani, *Sens. Actuators B*, 110 (2005) 239
40. P. Norouzi, M.R. Ganjali, and P. Matloobi, *Electrochem. Commun.*, 7 (2005) 333
41. P. Norouzi, M.R. Nabi Bidhendi, M.R. Ganjali, A. Sepehri, and M. Ghorbani, *Microchim. Acta*, 152 (2005) 123
42. D. Velayutham and M. Noel, *Electrochim. Acta*, 36 (1991) 2031
43. S.A. Campbell and L.M. Peter, *J. Electroanal. Chem.* 306 (1991) 185
44. A.B. Velichenko and L.N. Nischeryakova, *Electrochim. Acta*, 39 (1994) 1603
45. A.Salkind, T. Atwater, P. Singh, S. Nelatury, S. Damodar, C. Fennie Jr and D. Reisner, *J. Power Sources*, 96 (2001) 151
46. A.Kirchev, A. Delaille, M. Perrin, E. Lemaire and F. Mattera, *Journal of Power Sources*, 170 (2007) 495
47. W.R. Osório, L.C. Peixoto and A. Garcia, *Journal of Power Sources*, 194 (2009) 1120
48. S. Ghasemi, M.F. Mousavi, H. Karami, M. Shamsipur and S.H. Kazemi, *Electrochimica Acta*, 52 (2006) 1596
49. I.Petersson, B. Berghult and E. Ahlberg, *J. Power Sources*, 74 (1998) 98
50. D. Pavlov and G. Petkova, *J. Electrochem. Soc.*, 149 (2002) A654
51. H.S. Panesar, *J. Power Sources*, 3 (1971) 79
52. J.G. Sunderland, *J. electroanal Chem*, 71 (1976) 341
53. V. Dane1 and V. Plichon, *Electrochim. Acta*, 28 (1983) 781
54. J.P. Carr, N.A. Hampson and R. Taylor, *J. electroanal Chem*, 33 (1971) 109
55. S. Fletcher and D.B. Matthews, *J. appl. Electrochem*, 11 (1981) 11
56. R. Ponraj, S.D. McAllister, F. Cheng and D.B. Edwards, *J. Power Source*, 189 (2009) 1199